crystals

MDPI

Article

Nanoarchitectonics and Molecular Docking of 4-(Dimethylamino)Pyridin-1-Ium 2-3 Methyl-4-Oxo-Pyri-Do[1,2-*a*]Pyrimidine-3-Carboxylate

Sanae Lahmidi [1,*], El Hassane Anouar [2,*], Walid Ettahiri [3], Mohamed El Hafi [1], Fatima Lazrak [4], Mohammed M. Alanazi [5], Ashwag S. Alanazi [6], Mohamed Hefnawy [5], El Mokhtar Essassi [1] and Joel T. Mague [7]

1 Laboratory of Heterocyclic Organic Chemistry, Department of Chemistry, Faculty of Sciences, Mohammed V University in Rabat, Rabat 10106, Morocco; elhafi.mohamed1@gmail.com (M.E.H.); emessassi@yahoo.fr (E.M.E.)
2 Department of Chemistry, College of Science and Humanities in Al-Kharj, Prince Sattam Bin Abdulaziz University, Al-Kharj 11942, Saudi Arabia
3 Laboratory of Electrochemistry, Modelisation and Environment Engineering, Department of Chemistry, Faculty of Sciences Dhar El Mahraz, Sidi Mohamed Ben Abdellah University in Fez, Fez 30000, Morocco; walidtahiri4@gmail.com
4 Laboratory of Medicinal Chemistry, Drug Sciences Research Center, Faculty of Medicine and Pharmacy, Mohammed V University in Rabat, Rabat 10106, Morocco; f.lazrak@um5r.ac.ma
5 Department of Pharmaceutical Chemistry, College of Pharmacy, King Saud University, Riyadh 11451, Saudi Arabia; mmalanazi@ksu.edu.sa (M.M.A.); mhefnawy@ksu.edu.sa (M.H.)
6 Department of Pharmaceutical Sciences, College of Pharmacy, Princess Nourah Bint Abdulrahman University, Riyadh 11671, Saudi Arabia; asalanzi@pnu.edu.sa
7 Department of Chemistry, Tulane University, New Orleans, LA 70118, USA; joelt@tulane.edu
* Correspondence: lahmidi_sanae@yahoo.fr (S.L.); anouarelhassane@yahoo.fr (E.H.A.)

check for updates

Citation: Lahmidi, S.; Anouar, E.H.; Ettahiri, W.; El Hafi, M.; Lazrak, F.; Alanazi, M.M.; Alanazi, A.S.; Hefnawy, M.; Essassi, E.M.; Mague, J.T. Nanoarchitectonics and Molecular Docking of 4-(Dimethylamino)Pyridin-1-Ium 2-3 Methyl-4-Oxo-Pyri-Do[1,2-*a*]Pyrimidine-3-Carboxylate. *Crystals* **2023**, *13*, 1333. https://doi.org/10.3390/cryst13091333

Academic Editors: Saied M. Soliman, Assem Barakat and Ayman El-Faham

Received: 27 July 2023
Revised: 27 August 2023
Accepted: 29 August 2023
Published: 31 August 2023

Copyright: © 2023 by the authors. Licensee MDPI, Basel, Switzerland. This article is an open access article distributed under the terms and conditions of the Creative Commons Attribution (CC BY) license (https://creativecommons.org/licenses/by/4.0/).

Abstract: A retro-Claisen reaction of 1-(4-oxo-4H-pyrido [1,2-*a*]pyrimidin-3-yl)butane-1,3-dione, **3**, in the presence of potassium hydroxide and 4-dimethylamino-pyridine has been carried out, leading to 4-(dimethylamino)pyridin-1-ium 2-methyl-4-oxo-pyrido [1,2-*a*]pyrimidine-3-carboxylate **5**. A plausible mechanism explaining the formation of the title compound has been proposed. A single-crystal X-ray diffraction analysis confirms the crystal structure of the isolated organic salt (**5**). In the crystal, the title compound adopts a layered structure where there are stacks of cations and anions formed by slipped π-stacking interactions. These stacks are linked by regions consisting of water molecules that are hydrogen-bonded together. DFT and Hirshfeld surface analysis supported the experimental results of the molecular geometry and the intercontacts between different units in the crystal. The druglikeness, ADMET properties, and predicted targets were investigated, and the observed results suggest that **5** may act as a carbonic anhydrase I inhibitor. The assumption is confirmed by docking **5** into the active binding site of carbonic anhydrase, which shows it to have good binding affinities and to form stable complexes with the active residues of carbonic anhydrase I.

Keywords: alkaline cleavage; retro-Claisen; β-diketones; X-ray diffraction; DFT; molecular docking; ADMET

1. Introduction

Numerous N-heterocyclic compounds are found in a wide variety of biologically active substances [1–5]. These include vitamins, nucleic acids, antibiotics, pharmaceuticals, agrochemicals, and more. Furthermore, nitrogen heterocycles are present in almost 75% of known small-molecule drugs. A multitude of nitrogen-containing heterocyclic compounds exhibit a broad spectrum of pharmacological properties, making them promising building blocks for the construction of new drug candidates. This is due to the nitrogen atom's

capacity to readily form hydrogen bonds with biological targets [6–8], its ability to donate or accept protons, and its ability to easily form various weak interactions.

Pyridopyrimidines are a significant group of nitrogen-containing heterocycles possessing a diverse range of biological activities. Moreover, pyrido[1,2-*a*]pyrimidine constitutes the core structure of some marketed drugs, including Seganserin, an antihypertensive [9], Barmastine, an antiallergic agent [10], Pemirolast, an antiallergic agent [11], Pirenperone, a tranquilizer [12], Lusaperidone, an antidepressant [13] and Ramastine, an antiallergic, anti-ulcerative, and antiasthmatic agent (Figure 1) [10,12–16].

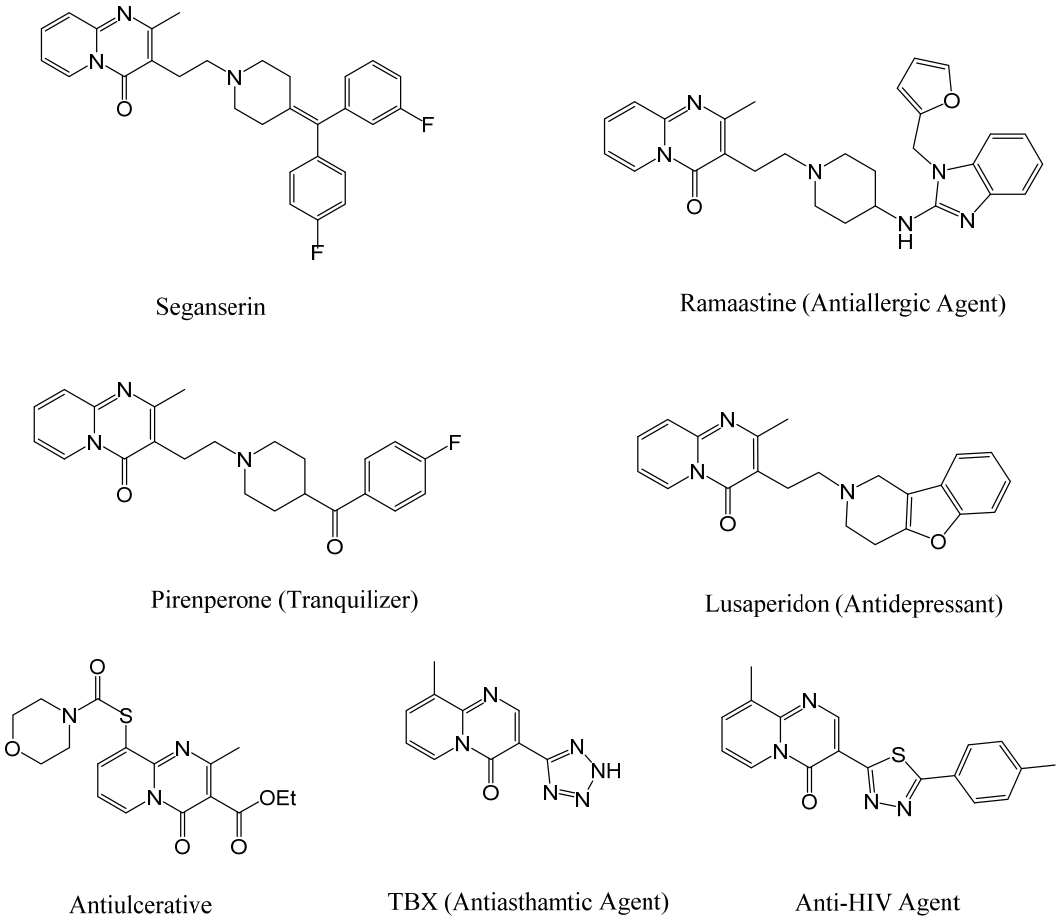

Figure 1. Biologically active 4H-pyrido[1,2-*a*]pyrimidin-4-ones.

2. Results and Discussion

2.1. Mechanism of the Synthesis of 4-(Dimethylamino)Pyridin-1-Ium 2-Methyl-4-Oxo-Pyrido[1,2-a Pyrimidine-3-Carboxylate

The retro-Claisen reaction, a useful synthetic tool in organic chemistry, leads to carboxylic acid derivatives involving a β-dicarbonyl carbon–carbon bond cleavage under various conditions [17,18]. Continuing our previous investigations on the synthesis of pyrido[1,2-*a*]pyrimidine derivatives [19,20], we describe the alkaline cleavage of 1-(4-oxo-4H-pyrido[1,2-*a*]pyrimidin-3-yl)butane-1,3-dione (**3**), which acts as an unsymmetrical β-diketone. This cleavage was carried out using potassium hydroxide and 4-dimethylaminopyridine as bases under refluxing conditions in ethanol. The unsymmetrical β-diketone used in this study was prepared by condensing 3-acetyl-4-hydroxy-6-methyl-2H-pyran-2-one, **1**, with 2-aminopyridine, **2**, in refluxing *n*-butanol according to a synthetic route developed by our team [21]. Compound **3** can exist in two tautomeric forms, **3a** and **3b**, and was reacted with a mixture of potassium hydroxide and 4-dimethylaminopyridine

in refluxing ethanol to produce 4-dimethylaminopyridin-1-ium 2-methyl-4-oxo-pyrido[1,2-*a*]pyrimidine-3-carboxylate, **5**, as depicted in Scheme 1.

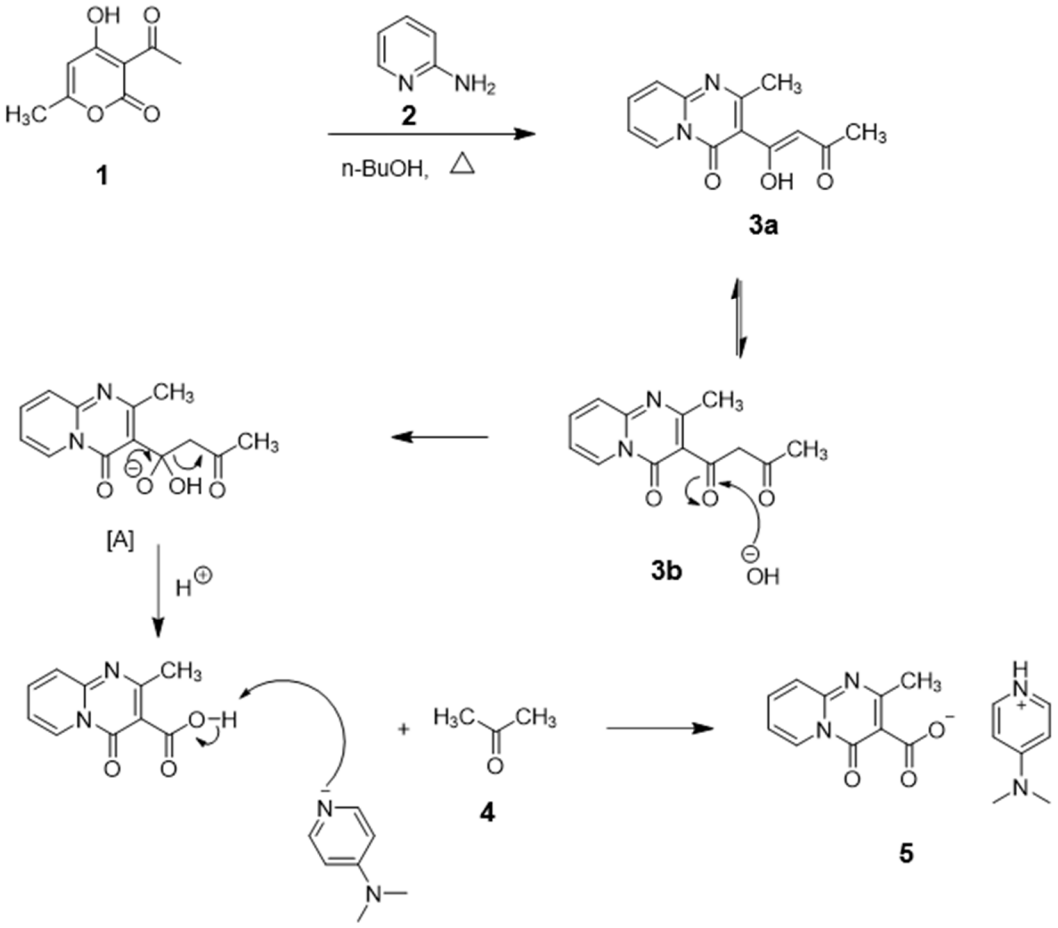

Scheme 1. A plausible mechanism for the formation of 4-(dimethylamino)pyridin-1-ium 2-methyl-4-oxo-pyrido[1,2-*a*]pyrimidine-3-carboxylate **5**.

A proposed mechanism suggests that the formation of **5** involves a nucleophilic attack by a hydroxide ion on the ketonic carbonyl attached to the pyridinic carbon in the 3-position of the biheterocyclic system, resulting in the formation of an intermediate [A]. The latter then undergoes a carbon–carbon bond cleavage, leading to the formation of the carboxylic acid [B]. The carboxylic acid subsequently reacts with 4-dimethylaminopyridine to yield the organic salt **5** (Scheme 1).

2.2. X-ray Analysis

The geometrical parameters for the cation and the anion are as expected for the given formulation. In the crystal, the ions stack along the normal to $(10\bar{2})$ in the order cation-anion-anion-cation as the repeat unit. These are formed by slipped π-stacking interactions between cation pyridinium and anion pyrimidine rings (centroid···centroid = 3.5041(5) Å, dihedral angle = 3.74(4)°, slippage = 1.10 Å) and between anion pyrido and anion pyrimidine rings (centroid···centroid = 3.6680(5) Å, dihedral angle = 3.70(4)°, slippage = 1.54 Å) (Figure 2). The solvent water molecules form hydrogen-bonded regions between the stacks and connect them (Table 1 and Figure 2).

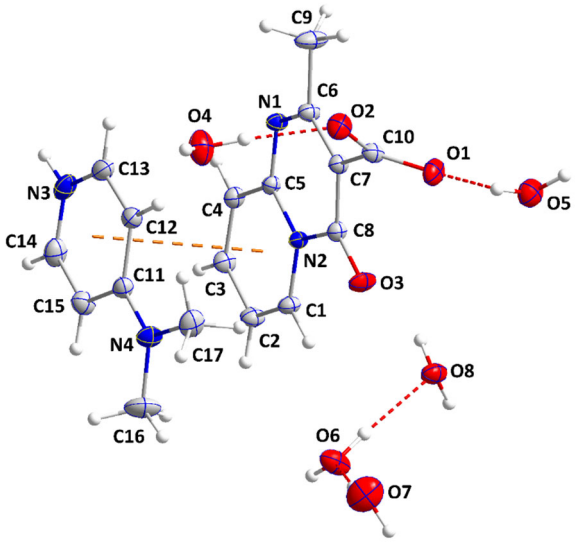

Figure 2. The structure of **5** consists of an asymmetric unit, which is shown with a labeling scheme and 50% probability ellipsoids. The hydrogen bonds formed by O—H···O interactions and the slipped π-stacking interactions are depicted with red and orange dashed lines, respectively. The disordered water molecules are only shown for the major components.

Table 1. Hydrogen bonds (Å,°) for **5**.

D—H···A	D—H	H···A	D···A	D—H···A
C1—H1···O6	0.95	2.57	3.2568 (11)	130
C2—H2···O2 [i]	0.95	2.51	3.3905 (10)	154
N3—H3A···O1 [ii]	0.91	2.17	2.9118 (10)	138
N3—H3A···O3 [ii]	0.91	2.15	2.8662 (10)	135
C12—H12···O4	0.95	2.44	3.3663 (11)	164
C13—H13···O6 [iii]	0.95	2.58	3.5143 (11)	168
C14—H14···O7 [ii]	0.95	2.54	3.2957 (14)	137
O4—H4A···O7 [iv]	0.87	1.89	2.7427 (12)	165
O4—H4B···O2	0.87	1.90	2.7713 (10)	175
O5—H5A···O1	0.87	1.92	2.7831 (10)	170
O5—H5B···O8 [v]	0.87	1.93	2.7944 (10)	172
O5—H5C···O5 [v]	0.87	1.98	2.8259 (15)	164
O6—H6A···O8	0.87	1.93	2.7975 (10)	176
O6—H6B···O1 [i]	0.87	1.91	2.7705 (9)	172
O7—H7A···O4 [vi]	0.87	1.95	2.8018 (13)	167
O7—H7B···O6	0.87	1.84	2.7058 (10)	173
O8—H8A···N1 [vii]	0.87	1.98	2.8457 (9)	179
O8—H8B···O8 [viii]	0.87	1.91	2.7716 (13)	170
O8—H8C···O5 [v]	0.87	1.93	2.7944 (10)	176

The following are the symmetry codes for the structure: (i) x, y − 1, z; (ii) x − 1, y, z; (iii) x − 1, y + 1, z; (iv) −x + 1, −y + 1, −z + 1; (v) −x + 2, −y + 1, −z; (vi) x + 1, y − 1, z; (vii) −x + 1, −y + 1, −z; (viii) −x + 2, −y, −z.

2.3. DFT Results

The optimized structure of 4-(dimethylamino)pyridin-1-ium 2-methyl-4-oxo-4*H*-pyrido[1,2-*a*]pyrimidine-3-carboxylate by itself is illustrated in Figure 3a. The comparison of the X-ray and optimized structures in Figure 3c shows that the calculated bond distances, bond angles, and dihedral angles are in good agreement with the experimental data. In the X-ray structure (Figure 3b), the interaction between the two ions occurs through π-stacking interactions (Figure 3b). However, the optimization only considered the two ions in the gas phase and did so in the absence of the hydration waters. With their absence, their hydrogen bonding to the ions is not included in the calculations, and

two hydrogen bonds are formed between the carboxylate group lone pairs in the 2-methyl-4-oxo-4*H*-pyrido[1,2-*a*]pyrimidine-3-carboxylate anion and the aromatic C–H units of the 4-(dimethylamino)pyridin-1-ium cation (Figure 3a), suggesting that these interactions outweigh π-stacking interactions in this scenario. Table 2 presents the selected experimental and calculated geometrical parameters of 4-(dimethylamino)pyridin-1-ium 2-methyl-4-oxo-4*H*-pyrido[1,2-*a*]pyrimidine-3-carboxylate. The discrepancies between the experimental and calculated bond lengths, bond angles, and torsion angles are not significant, with the maximum differences being less than 0.02 Å, 10.55, and 7 degrees, respectively. These minor variations are consistent with the superposition in Figure 3c.

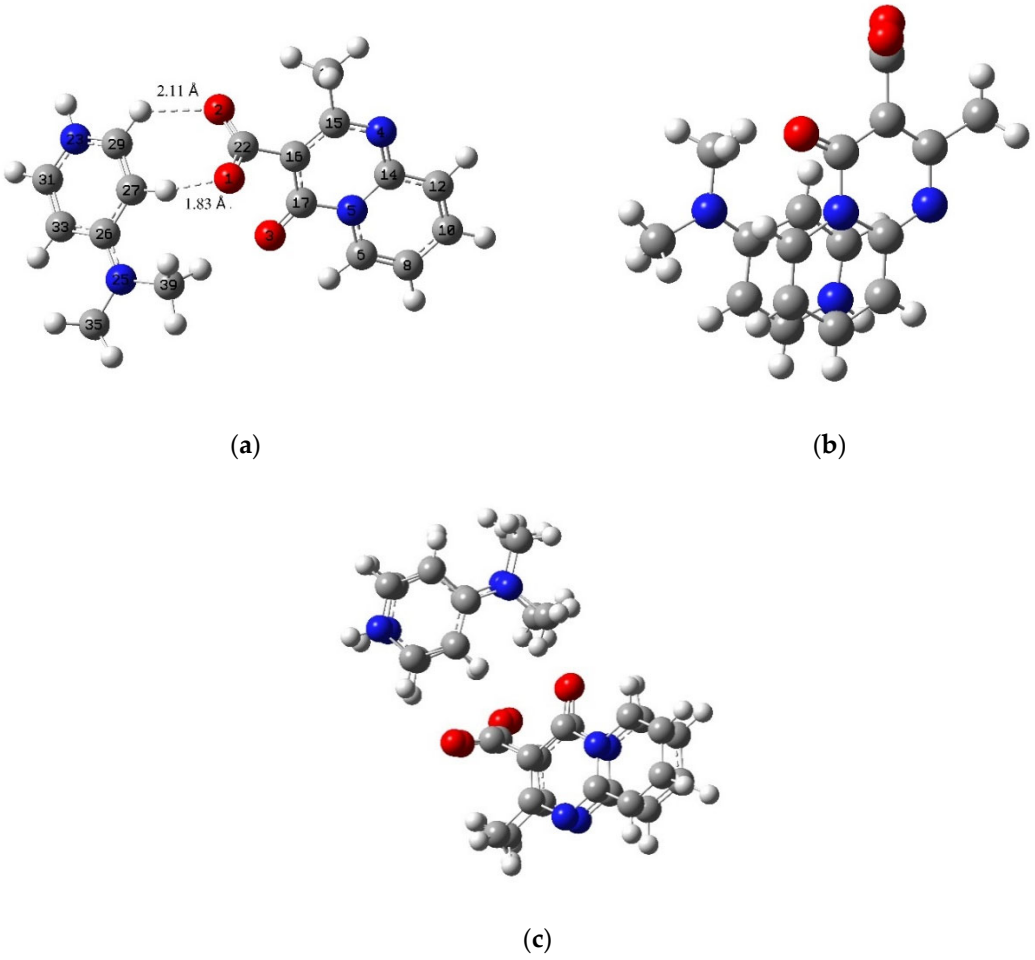

Figure 3. (**a**) The optimized structure of **5**, (**b**) X-ray geometries of **5**, and (**c**) their superposition.

Table 2. The selected experimental and optimized structure parameters of **5**.

Bond Lengths (Å)				Bond Angles (°)			
	Cal	**X-ray**	**ΔL(Å)**		**Cal**	**X-ray**	**ΔA (°)**
O1-C22	1.265	1.259 (4)	0.01	O1-C22-O2	125.15	128.43 (8)	3.29
O2-C22	1.244	1.259 (2)	0.01	O1-C22-C16	125.15	114.59 (9)	10.55
C16-C22	1.514	1.530 (3)	0.02	O3-C17-C16	127.44	128.82 (6)	1.39
O3-C17	1.233	1.233 (5)	0.00	C17-N5-C14	121.18	121.31 (8)	0.13
N4-C14	1.330	1.318 (7)	0.01	N5-C14-N4	122.43	122.61 (9)	0.19
N5-C14	1.381	1.398 (5)	0.02	C26-N25-C39	123.00	119.66 (9)	3.33
N23-C29	1.351	1.365 (4)	0.01	O1-C22-C16-C15	−124.14	−118.98 (6)	5.15
N23-C31	1.346	1.359 (0)	0.01	O1-C22-C16-C17	57.03	60.86 (8)	3.83

Table 2. *Cont.*

	Bond Lengths (Å)				Bond Angles (°)		
	Cal	**X-ray**	**ΔL(Å)**		**Cal**	**X-ray**	**ΔA (°)**
N25-C26	1.338	1.346 (6)	0.01	O3-C17-C16-C22	−2.97	3.78 (4)	6.75
N25-C35	1.462	1.458 (6)	0.00	C6-N5-C17-O3	3.41	−2.28 (6)	5.70
N25-C39	1.459	1.477 (0)	0.02	C27-C26-N25-C39	−1.99	−1.99 (2)	0.00
C26-C27	1.424	1.422 (3)	0.00	C27-C26-N25-C35	−176.34	−176.34 (1)	0.00
C27-C29	1.367	1.366 (2)	0.00	C33-C26-N25-C35	4.16	4.15 (8)	0.00

2.4. Hirshfeld Surface Analysis

The hydrogen bonding pattern of the HS of **5** mapped over d_{norm} is illustrated in Figure 4. The figure shows that strong intermolecular hydrogen bonds are formed between the lone pairs of the carboxylate groups of 2-methyl-4-oxo-4*H*-pyrido[1,2-*a*]pyrimidine-3-carboxylate and the NH and CH of the 4-(dimethylamino)pyridin-1-ium cation, with lengths of 2.081 and 2.883 Å, respectively.

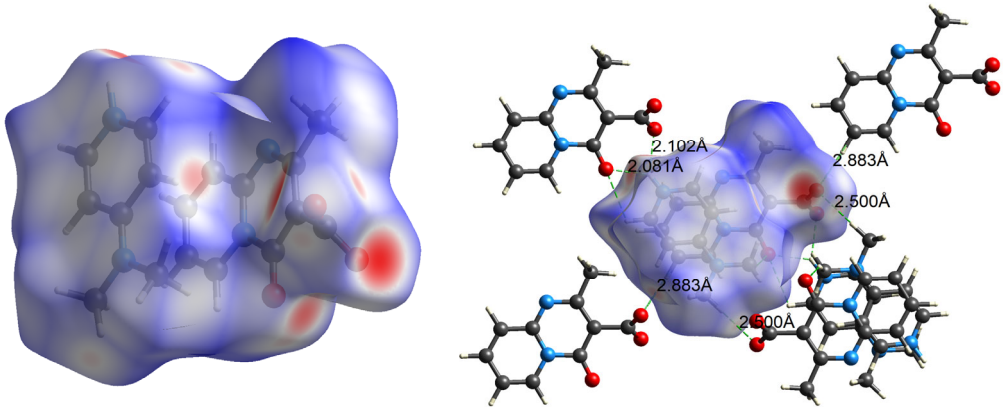

Figure 4. d_{norm} mapped on the Hirshfeld surface of **5**.

Figure 5 shows the electrostatic potential of **5**, with the CO groups located in the red region indicating that they act as hydrogen bond acceptors. The amine group is located in the blue region, indicating that it acts as a hydrogen bond donor.

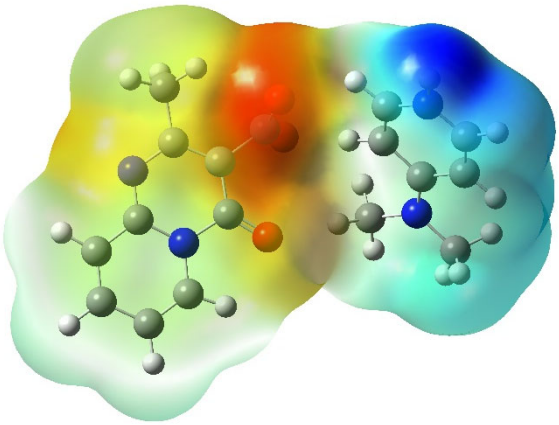

Figure 5. ESP of **5**.

Figure 6 displays the 2D fingerprint plots of **5**, which show that the most prevalent interatomic contacts between the units of **5** were hydrogen atoms (H···H, accounting for 50.5% of the total) and hydrogen bonds O···H/H···O (accounting for 31.7% of the total).

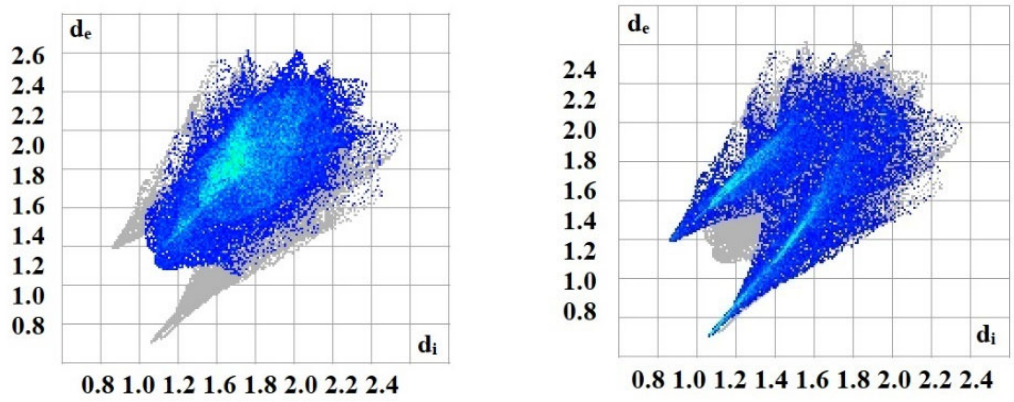

Figure 6. The two-dimensional fingerprint plots showing the major intercontacts H···H (**left**) and O···H/H···O (**right**) in **5**.

2.5. ADMET and Druglikeness Prediction of **5**

The supplementary material contains the calculated ADMET properties of **5**, as well as its anionic (F1) and cationic (F2) components, which are presented in Tables S1–S5. These show that **5** adheres to Lipinski's rule of five and has a lipophilicity value (MlogP) of 0.68, which is lower than the threshold of 4.15 (Tables S2 and S5), indicating good druglikeness properties. The topological surface area (TPSA) of **5** was calculated to be between 78–125 Å^2 (Table S1). This suggests that the compound is likely to be orally absorbed, and its bioavailability score of 0.55 (Table S5) further supports this conclusion. The bioavailability of **5** is also visualized using bioavailability radars (Figure 7), which show that **5** falls within the pink area of the polygon, except for the unsaturation parameter, which is still within the polygon but outside the pink area. This suggests that **5** may have a good oral bioavailability (Figure S1). The pharmacokinetic properties in Table S4 indicate that **5** has a high gastrointestinal (GI) absorption, and the lack of penetration through the Blood–Brain Barrier (BBB) is shown in Figure 8. To predict the potential biological targets of **5**, a pie chart was generated, which suggests that **5** may function as an inhibitor of carbonic anhydrase I (Figure 9).

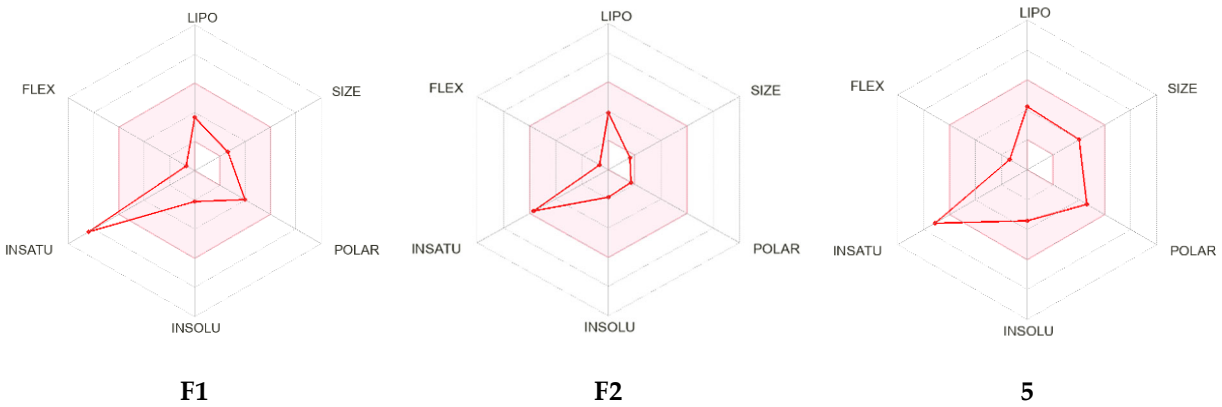

Figure 7. Bioavailability radars of **5** and its anionic **F1** and cationic **F2** components.

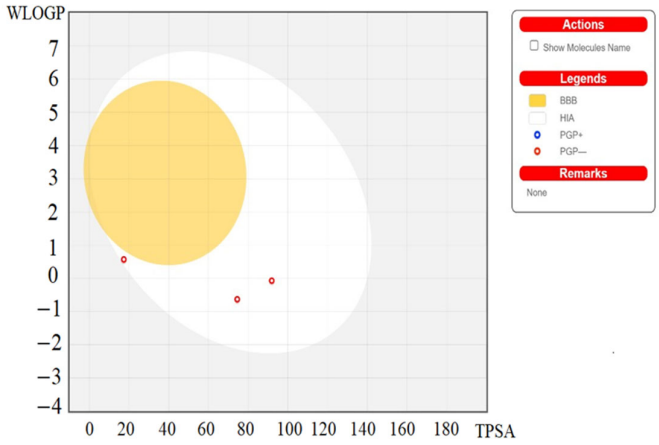

Figure 8. Boiled-egg model of **5** and its anionic **F1** and cationic **F2** components.

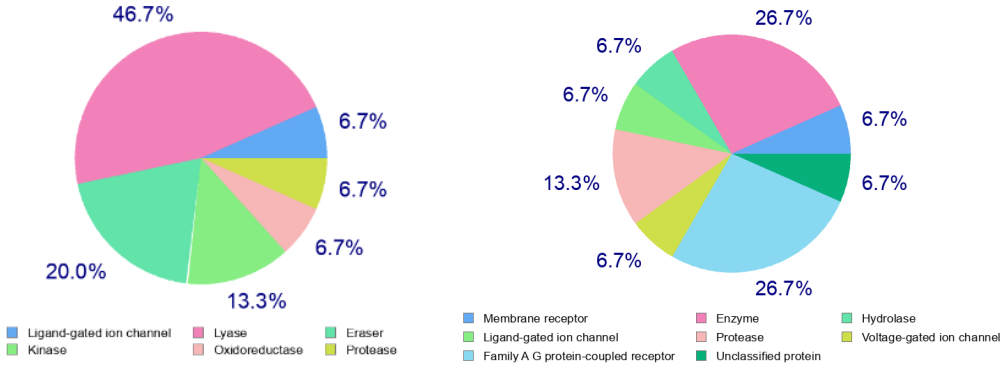

Figure 9. Predicted biological targets of anionic **F1** and cationic **F2** components of **5**.

2.6. Molecular Docking Study

To validate the potential inhibitory effect of **5** on carbonic anhydrase I (CAI), a docking study was conducted, which examined the binding affinity of the individual components of **5** with the CAI binding site. Table 3 presents the binding energies of the **F1**-DNA-PK and **F2**-DNA-PK complexes, the number of hydrogen bonds formed between the docked molecules and the active site residues of CAI, and the number of amino acids in closest proximity to the docked compounds.

Table 3. Binding energies, hydrogen bonds, and the number of closest residues to the docked components **F1** and **F2** of **5**.

	Free Binding Energy (kcal/mol)	H-Bonds (HBs)	Number of Closest Residues to the Docked Ligand in the Active Site *
F1	−5.54	3	7
F2	−3.72	1	5

* displays the number of amino acids in the active site of carbonic anhydrase I that interact with **F1** and **F2**.

Both **F1** and **F2** components of **5** are able to fit into the binding site of carbonic anhydrase I with relative ease and form stable complexes with its amino acids, as evidenced by their binding energies of −5.54 and −3.72 kcal-mol^{-1} for **F1**-CAI and **F2**-CAI, respectively. The negative binding energies suggest that the inhibition of carbonic anhydrase I by **5** is thermodynamically favorable and occurs spontaneously. Figure 10 illustrates the 2D and 3D binding interactions between **F1** and **F2** with the amino acids located in the binding site of CAI. The results presented in Table 3 and Figure 10 suggest that the binding affinity of **5** with the CAI binding site is primarily attributed to **F1**. This is supported by the observation

that the **F1**–CAI complex is more stable, which could be due to the higher number of hydrogen bonds formed between **F1** and the amino acids HIS A119 and THR A199 of CAI. Specifically, the acetate group in **F1** establishes three hydrogen bonds with THR199 and HIS A199 at distances of 2.85, 2.93, and 3.05 Å (i.e., these distances are between the non-hydrogen components of the interactions), respectively (Figure 10).

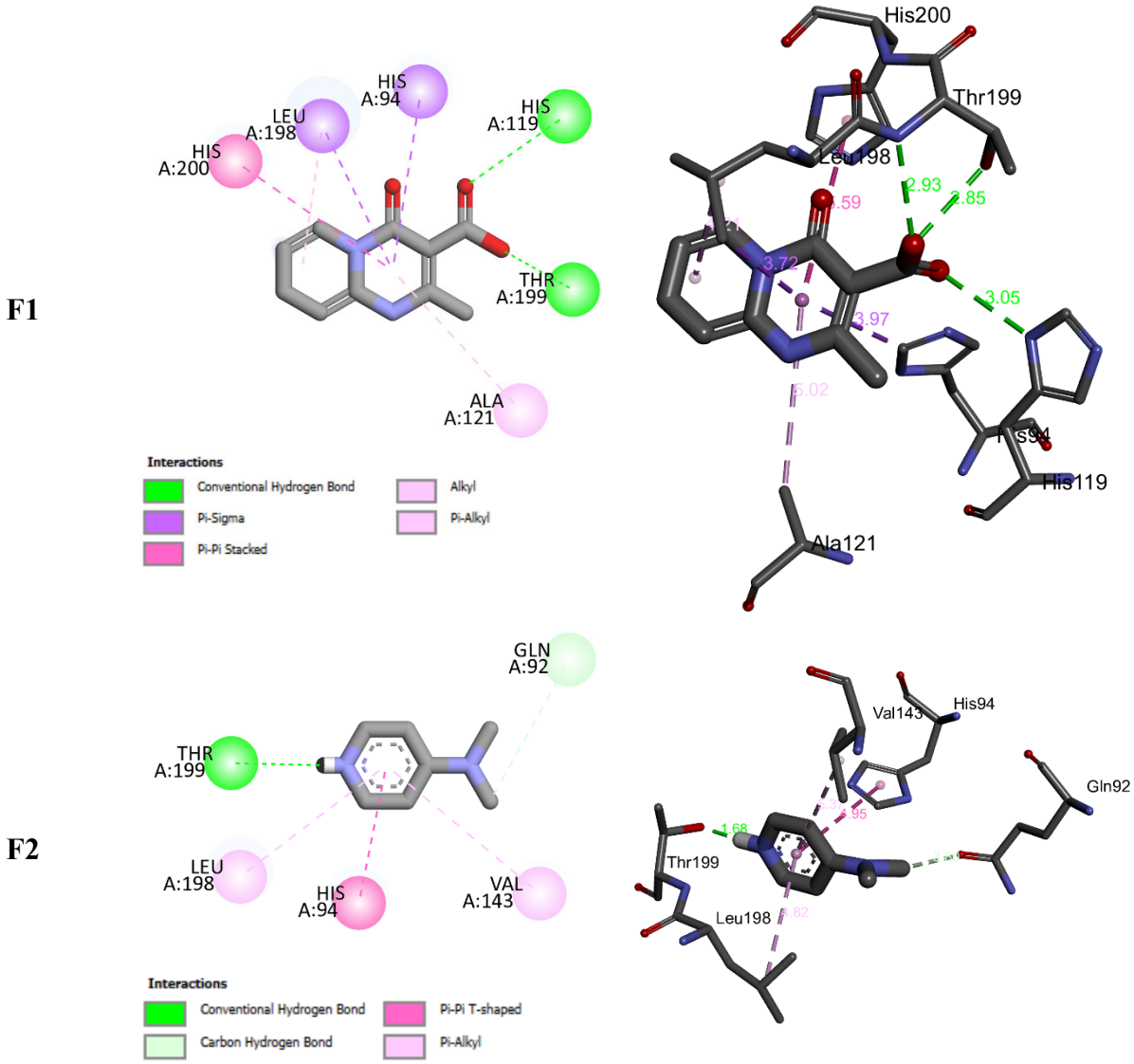

Figure 10. 2D and 3D closest interactions between the active site residues of carbonic anhydrase I and units of **5**.

3. Materials and Methods

3.1. General Procedure

A solution containing 0.01 mol of 3-acetyl-4-hydroxy-6-methyl-2H-pyran-2-one **1** and 0.01 mol of 2-aminopyridine **2** was refluxed in butanol for 24 h. Upon removal of the reaction solvent under reduced pressure, the product is pyridopyrimidine **3**, which exists in two tautomeric forms, **3a** and **3b**.

A solution containing a mixture of pyrido[1,2-*a*]pyrimidine **3** (1.5 g, 6.14 mmol), 0.1 mol of 4-dimethylaminopyridine **4**, and potassium hydroxide (0.51 g, 9.21 mmol) in 30 mL of ethanol was stirred under reflux for 6 h. The reaction mixture was allowed to cool to room temperature, and the resulting residue was extracted with 15 mL of dichloromethane, followed by removal of the solvent under reduced pressure. The resulting

solid was then recrystallized from diethyl ether, yielding the organic salt **5** as white crystals in a 60% yield (Scheme 2).

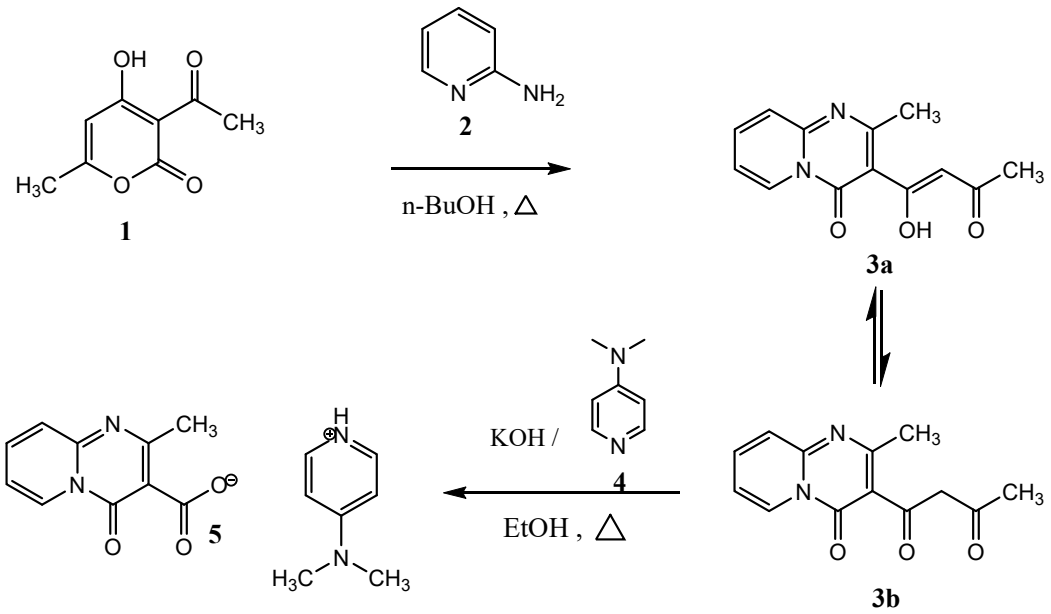

Scheme 2. Synthesis scheme of **5**.

3.2. X-ray Crystallography

For the X-ray crystallographic analysis, a colorless, thick plate-like sample of $C_{17}H_{28}N_4O_8$ with approximate dimensions of 0.147 × 0.272 × 0.275 mm was used. X-ray intensity data were collected using a Bruker D8 QUEST PHOTON 3 diffractometer system equipped with a fine-focus sealed tube (MoKα, λ = 0.71073 Å) and a graphite monochromator, controlled by the APEX4 software [22]. The initial data obtained were transformed into F^2 values using SAINT [22], which also conducted a global refinement of the unit cell parameters. A numerical absorption correction and merging of equivalent reflections was performed by SADABS [22].

The structure was solved by dual space methods (SHELXT) and refined on F^2 by full-matrix, least-squares procedures (SHELXL). Hydrogen atoms attached to carbon were included as riding contributions in idealized positions, with isotropic displacement parameters tied to those of the attached atoms. Those bound to nitrogen were located in difference maps and refined with DFIX 0.91 0.01 instructions. Details of data collection and refinement are provided in Table 4.

3.3. Hirshfeld Surface Analysis

Compound **5** was analyzed with Crystal Explorer 3.0, where both the Hirshfeld surface (HS) and 2D fingerprint plots were calculated [23,24]. The HS of **5** was visualized with d_{norm} values ranging from −0.11 to 1.19 au, with the blue color indicating lower values and red color indicating higher values. Additionally, the 2D fingerprint plots were displayed with an expanded scale ranging from 0.6 to 2.8 Å.

3.4. DFT Calculations

The Gaussian 16 software package was used to optimize the starting geometry of **5** at the B3LYP/6-311++G(d,p) level of theory [25]. To ensure that the optimized geometry obtained was a stable configuration, frequency calculations were carried out [26]. The input Z-matrix parameters for the DFT calculations were obtained from the X-ray coordinates of **5**, and the ESP surface and FMOs were computed using the same level of theory. The polarizable continuum model (PCM) was employed to account for solvent effects [27]. All DFT calculations were carried out using the Gaussian 16 software package [25].

Table 4. Crystal and refinement data for **5**.

Chemical Formula	**$C_{10}H_7N_2O_3 \cdot C_7H_{11}N_2 \cdot 5(H_2O)$**
M_r	416.43
Crystal system, space group	Triclinic, **$P\bar{1}$**
Temperature (K)	150
a, b, c (Å)	9.4302 (3), 9.7094 (3), 12.9484 (4)
α, β, γ (°)	77.686 (2), 71.945 (2), 66.414 (1)
V (Å^3)	1027.60 (6)
Z	2
Radiation type	Mo $K\alpha$
μ (mm^{-1})	0.11
Crystal size (mm)	0.28 × 0.27 × 0.15
Data collection	
Diffractometer	Bruker D8 QUEST PHOTON 3 diffractometer
Absorption correction	Numerical *SADABS* (Krause et al., 2015)
T_{min}, T_{max}	0.94, 0.98
No. of measured, independent andobserved [$I > 2\sigma(I)$] reflections	68,565, 7857, 6719
R_{int}	0.026
(sin $\theta/\lambda)_{max}$ (Å^{-1})	0.771
Refinement	
$R[F^2 > 2\sigma(F^2)]$, $wR(F^2)$, S	0.042, 0.119, 1.03
No. of reflections	7857
No. of parameters	267
H-atom treatment	H-atom parameters constrained
$\Delta\rho_{max}$, $\Delta\rho_{min}$ (e Å^{-3})	0.49, −0.25

3.5. In Silico ADMET and Druglikeness Properties

Compound **5** was subjected to ADMET (absorption, distribution, metabolism, excretion, and toxicity), druglikeness, pharmacokinetics, and physico-chemical property predictions using the Swiss ADME tool, which is available at http://www.swissadme.ch/ (accessed on 1 January 2023). In addition, the Swiss target prediction tool (http://www.swisstargetprediction.ch/ accessed on 1 March 2023) was used to predict the probable targets of **5** (accessed on 1 January 2023).

3.6. Molecular Docking Study

Based on the predictions from ADMET and druglikeness analysis, it is indicated that **5** has the potential to act as an inhibitor for carbonic anhydrase I. To investigate the feasibility of this approach, a molecular docking study was carried out using the Autodock software package [28] to dock **5** into the binding site of carbonic anhydrase I. The target enzyme and original docked ligand were obtained from the RCSB website (PDB code 2NN7) [29]. The accuracy of the molecular docking study was validated by re-docking the original ligand into the binding site, which resulted in an RMSD of 1.30 Å and a binding energy of −6.93 kcal-mol^{-1}. For additional information regarding the docking of **5** and the original ligand, please refer to our previous publication [30].

4. Conclusions

In this work, we report an interesting alkaline cleavage involving a retro-Claisen reaction of 3-acetoacetyl-2-methyl-pyrido[1,2-a]pyrimidin-4-one in the presence of potassium hydroxide and 4-dimethylaminopyridine as bases, leading to 4-(dimethylamino)pyridin-1-ium 2-methyl-4-oxo-pyrido[1,2-a]pyrimidine-3-carboxylate, **5**. A plausible mechanism for the formation of **5** has been proposed. The crystal structure of **5** was determined by single-crystal X-ray diffraction analysis. The geometrical parameters for the cation and the

anion are as expected for the given formulation. In the crystal, the ions stack along the normal to $(10\bar{2})$ in the order cation-anion-anion-cation as the repeat unit. The intercontacts were determined through the analysis of Hirshfeld surface (HS) and 2D fingerprint plots. The structural parameters of **5** are relatively well reproduced by DFT calculations. The predicted ADMET, druglikeness, pharmacokinetics, and physico-chemical properties indicate that **5** may act as an inhibitor of carbonic anhydrase I, which is confirmed by its binding affinity using a molecular docking study.

Supplementary Materials: The following supporting information can be downloaded at: https://www.mdpi.com/article/10.3390/cryst13091333/s1, Table S1: Physicochemical Properties of **3** and **4**; Table S2: Lipophilicity of **3** and **4**; Table S3: Water Solubility of **3** and **4**; Table S4: Pharmacokinetics Properties of **3** and **4**; Table S5: Druglikeness Properties of **3** and **4**; Table S6: Medicinal Properties of **3** and **4**.

Author Contributions: Conceptualization, S.L. and W.E.; methodology, F.L.; software, M.E.H. and J.T.M.; validation, S.L., E.H.A. and F.L.; formal analysis, M.M.A., M.H. and A.S.A.; investigation, S.L.; resources, M.M.A., M.H. and A.S.A.; data curation, J.T.M.; writing—original draft preparation, F.L., E.H.A. and S.L.; writing—review and editing, E.M.E.; visualization, S.L. and E.H.A.; supervision, E.M.E.; project administration, S.L.; funding acquisition, M.H. and A.S.A. All authors have read and agreed to the published version of the manuscript.

Funding: This work was funded by Princess Nourah bint Abdulrahman University Researchers Supporting Project number (PNURSP2023R342), Princess Nourah bint Abdulrahman University, Riyadh, Saudi Arabia. This work was also funded by the Researchers Supporting Project.

Data Availability Statement: Not applicable.

Acknowledgments: This work was funded by Princess Nourah bint Abdulrahman University Researchers Supporting Project number (PNURSP2023R342), Princess Nourah bint Abdulrahman University, Riyadh, Saudi Arabia. This work was also funded by the Researchers Supporting Project number (RSPD2023R754), King Saud University, Riyadh, Saudi Arabia.

Conflicts of Interest: The authors declare no conflict of interest.

Sample Availability: Not applicable.

References

1. Eftekhari-Sis, B.; Zirak, M.; Akbari, A. Arylglyoxals in synthesis of heterocyclic compounds. *Chem. Rev.* **2013**, *113*, 2958–3043. [CrossRef] [PubMed]
2. Kerru, N.; Maddila, S.; Jonnalagadda, S.B. Design of carbon-carbon and carbon-heteroatom bond formation reactions under green conditions. *Curr. Org. Chem.* **2019**, *23*, 3154–3190. [CrossRef]
3. Ju, Y.; Varma, R.S. Aqueous N-heterocyclization of primary amines and hydrazines with dihalides: Microwave-assisted syntheses of N-azacycloalkanes, isoindole, pyrazole, pyrazolidine, and phthalazine derivatives. *J. Org. Chem.* **2006**, *71*, 135–141. [CrossRef] [PubMed]
4. Zárate-Zárate, D.; Aguilar, R.; Hernández-Benitez, R.I.; Labarrios, E.M.; Delgado, F.; Tamariz, J. Synthesis of α-ketols by functionalization of captodative alkenes and divergent preparation of heterocycles and natural products. *Tetrahedron* **2015**, *71*, 6961–6978. [CrossRef]
5. Leeson, P.D.; Springthorpe, B. The influence of drug-like concepts on decision-making in medicinal chemistry. *Nat. Rev. Drug Discov.* **2007**, *6*, 881–890. [CrossRef]
6. Gallop, M.A.; Barrett, R.W.; Dower, W.J.; Fodor, S.P.; Gordon, E.M. Applications of combinatorial technologies to drug discovery. 1. Background and peptide combinatorial libraries. *J. Med. Chem.* **1994**, *37*, 1233–1251. [CrossRef]
7. Walsh, C.T. Nature loves nitrogen heterocycles. *Tetrahedron Lett.* **2015**, *56*, 3075–3081. [CrossRef]
8. Zhang, B.; Studer, A. Recent advances in the synthesis of nitrogen heterocycles via radical cascade reactions using isonitriles as radical acceptors. *Chem. Soc. Rev.* **2015**, *44*, 3505–3521. [CrossRef]
9. Pettersson, A.; Gradin, K.; Hedner, T.; Persson, B. Antihypertensive mechanism of action of ketanserin and some ketanserin analogues in the spontaneously hypertensive rat. *Naunyn-Schmiedebergs Arch. Pharmacol.* **1985**, *329*, 394–397. [CrossRef]
10. Awouters, F.; Vermeire, J.; Smeyers, F.; Vermote, P.; Van Beek, R.; Niemegeers, C.J. Oral antiallergic activity in ascaris hypersensitive dogs: A study of known antihistamines and of the new compounds ramastine (R 57 959) and levocabastine (R 50 547). *Drug Dev. Res.* **1986**, *8*, 95–102. [CrossRef]
11. Yanagihara, Y.; Kasai, H.; Kawashima, T.; Shida, T. Immunopharmacological studies on TBX, a new antiallergic drug (1) Inhibitory effects on passive cutaneous anaphylaxis in rats and guinea pigs. *Jpn. J. Pharmacol.* **1988**, *48*, 91–101. [CrossRef]

12. Smith, R.L.; Barrett, R.J.; Sanders-Bush, E. Neurochemical and behavioral evidence that quipazine-ketanserin discrimination is mediated by serotonin2A receptor. *J. Pharmacol. Exp. Ther.* **1995**, *275*, 1050–1057.
13. Kennis, L.; Bischoff, F.; Mertens, C.; Love, C. FAFV d. Keybus, MBS Pieters, AAHP Megens and JE Leysen. *Bioorg. Med. Chem. Lett.* **2002**, *10*, 71. [CrossRef]
14. Varga, M.; Kapui, Z.; Bátori, S.; Nagy, L.T.; Vasvári-Debreczy, L.; Mikus, E.; Urbán-Szabó, K.; Arányi, P. A novel orally active inhibitor of HLE. *Eur. J. Med. Chem.* **2003**, *38*, 421–425. [CrossRef] [PubMed]
15. Jeste, D.V.; Okamoto, A.; Napolitano, J.; Kane, J.M.; Martinez, R.A. Low incidence of persistent tardive dyskinesia in elderly patients with dementia treated with risperidone. *Am. J. Psychiatry* **2000**, *157*, 1150–1155. [CrossRef] [PubMed]
16. Yao, P.; Zhai, X.; Liu, D.; Qi, B.H.; Tan, H.L.; Jin, Y.C.; Gong, P. Synthesis and Antiproliferative Activitiy of Novel Diaryl Ureas Possessing a 4H-Pyrido [1, 2-a] pyrimidin-4-one Group. *Arch. Der Pharm. Int. J. Pharm. Med. Chem.* **2010**, *343*, 17–23. [CrossRef] [PubMed]
17. Hussein, M.; Huynh, V.; Hommelsheim, R.; Koenigs, R.; Nguyen, T. An efficient method for retro-Claisen-type C–C bond cleavage of diketones with tropylium catalyst. *Chem. Commun.* **2018**, *54*, 12970–12973. [CrossRef] [PubMed]
18. Jukic, M.; Sterk, D.; Casar, Z. Recent advances in the retro-Claisen reaction and its synthetic applications. *Curr. Org. Synth.* **2012**, *9*, 488–512. [CrossRef]
19. Lahmidi, S.; Sert, Y.; Şen, F.; El Hafi, M.; Ettahiri, W.; Gökce, H.; Essassi, E.M.; Mague, J.T.; Ucun, F. Synthesis, crystal structure, Hirshfeld surface analysis, spectral characterizations and quantum computational assessments of 1-hydroxy-3-methyl-11H-pyrido [2, 1-b] quinazolin-11-one. *J. Mol. Struct.* **2022**, *1249*, 131592. [CrossRef]
20. El Hafi, M.; Lahmidi, S.; Boulhaoua, M.; El Ghayati, L.; Albalwi, H.; Anouar, E.H.; Alharthi, A.I.; Mague, J.T.; Essassi, E.M.; Lai, C.H. A new synthetic route for the preparation of 2, 2′, 5′-trimethyl-7-oxo-4, 7-dihydro-[6, 7′-bipyrazolo [1, 5-a] pyrimidine]-3, 3′-dicarbonitrile, structural elucidation, Hirshfeld surface analysis, energy framework, density functional theory and molecular docking investigations. *J. Chin. Chem. Soc.* **2022**, *69*, 717–730.
21. Elotmani, B.; Elmahi, M.; Essassi, E.; Pierrot, M. 2-Méthyl-3-(3-méthyl-1H-pyrazol-5-yl) pyrido [1, 2-a] pyrimidin-4-one. *Acta Crystallogr. Sect. E Struct. Rep. Online* **2002**, *58*, o388–o389. [CrossRef]
22. Bruker AXS Inc. *APEX 3*; Bruker Advanced X-ray Solutions: Madison, WI, USA, 2016.
23. Spackman, P.R.; Turner, M.J.; McKinnon, J.J.; Wolff, S.K.; Grimwood, D.J.; Jayatilaka, D.; Spackman, M.A. CrystalExplorer: A program for Hirshfeld surface analysis, visualization and quantitative analysis of molecular crystals. *J. Appl. Crystallogr.* **2021**, *54*, 1006–1011. [CrossRef] [PubMed]
24. Turner, M.; McKinnon, J.; Wolff, S.; Grimwood, D.; Spackman, P.; Jayatilaka, D.; Spackman, M. *CrystalExplorer17*; University of Western Australia: Crawley WA, Australia, 2017.
25. Frisch, M.; Trucks, G.; Schlegel, H.; Scuseria, G.; Robb, M.; Cheeseman, J.; Scalmani, G.; Barone, V.; Petersson, G.; Nakatsuji, H. *Gaussian 16*; Gaussian, Inc.: Wallingford, CT, USA, 2016.
26. Andersson, M.P.; Uvdal, P. New scale factors for harmonic vibrational frequencies using the B3LYP density functional method with the triple-ζ basis set 6-311+ G (d, p). *J. Phys. Chem. A* **2005**, *109*, 2937–2941. [CrossRef] [PubMed]
27. Tomasi, J.; Persico, M. Molecular Interactions in Solution: An Overview of Methods Based on Continuous Distributions of the Solvent. *Chem. Rev.* **1994**, *94*, 2027–2094. [CrossRef]
28. Morris, G.M.; Huey, R.; Lindstrom, W.; Sanner, M.F.; Belew, R.K.; Goodsell, D.S.; Olson, A.J. AutoDock4 and AutoDockTools4: Automated docking with selective receptor flexibility. *J. Comput. Chem.* **2009**, *30*, 2785–2791. [CrossRef]
29. Srivastava, D.; Jude, K.M.; Banerjee, A.L.; Haldar, M.; Manokaran, S.; Kooren, J.; Mallik, S.; Christianson, D.W. Structural analysis of charge discrimination in the binding of inhibitors to human carbonic anhydrases I and II. *J. Am. Chem. Soc.* **2007**, *129*, 5528–5537. [CrossRef]
30. Karrouchi, K.; Fettach, S.; Anouar, E.H.; Bayach, I.; Albalwi, H.; Arshad, S.; Sebbar, N.K.; Tachalait, H.; Bougrin, K.; Faouzi, M.E.A.; et al. Synthesis, Spectroscopic Characterization, DFT, Molecular Docking and Antidiabetic Activity of N-Isonicotinoyl Arylaldehyde Hydrazones. *Polycycl. Aromat. Compd.* **2023**, *43*, 1469–1481. [CrossRef]

Disclaimer/Publisher's Note: The statements, opinions and data contained in all publications are solely those of the individual author(s) and contributor(s) and not of MDPI and/or the editor(s). MDPI and/or the editor(s) disclaim responsibility for any injury to people or property resulting from any ideas, methods, instructions or products referred to in the content.